VIC-Glacier (VIC-GL)

Model Calibration

VIC Generation 2 Deployment Report

Volume 5

Markus Schnorbus

Pacific Climate Impacts Consortium

University of Victoria

Victoria, BC

May 10, 2017

Citation

Schnorbus, M.A., 2018: *VIC Glacier (VIC-GL) – Model Calibration*, VIC Generation 2 Deployment Report, Volume 5, Pacific Climate Impacts Consortium, University of Victoria, Victoria, BC, 22 pp.

About PCIC

The Pacific Climate Impacts Consortium is a regional climate service centre at the University of Victoria that provides practical information on the physical impacts of climate variability and change in the Pacific and Yukon Region of Canada. PCIC operates in collaboration with climate researchers and regional stakeholders on projects driven by user needs. For more information see http://pacificclimate.org.

Disclaimer

Acknowledgements

The financial support of BC Hydro is gratefully acknowledged.

Table of Contents

List of Figures

List of Tables

1 Calibration Framework

Calibration of the VIC-GL model employs a multi-objective calibration paradigm. This approach exploits several different data sources in order to produce an optimized model based on explicitly constraining separate hydrologic processes. A multi-objective approach recognizes there are multiple ways in which a model can be best fit to the data. Hence, multi-objective problems tend not to have unique solutions. Using a Pareto-optimized set of parameters accepts that there is no "best" parameter set (model) and reflects uncertainty due to errors in the model structure, boundary conditions (i.e. meteorological data, hydrometric data, and soil, vegetation and topography parameters) and observations. Realizations of the parameter vectors that constitute the Pareto set will also reflect the choice of objective functions.

Consider a hydrologic modelling application in which we are given m observations x_j, $j = 1, \ldots, m$ of a hydrologic variable (e.g., streamflow), m model output values y_j, $j = 1, \ldots, m$ of the same variable, and n model parameters p_k, $k = 1, \ldots, n$. The Euclidean geometrical spaces of the observations and model output is $\mathbb{R}^m$ and that of the parameters is $\mathbb{R}^n$. Due to the presence of constraints acting on the model parameters, their domain is restricted to $P \subseteq \mathbb{R}^n$, the feasible parameter domain. Let us consider a single objective function h, such that (Cavazzuti 2013)

$$\begin{aligned} &\mathbf{g}(\mathbf{p}) : P \subseteq \mathbb{R}^n \longrightarrow Y \subseteq \mathbb{R}^m, \;\; y_k = g_k(\mathbf{p}), \;\; k = 1, \ldots, m \\ &f(\mathbf{p}) : P \subseteq \mathbb{R}^n \longrightarrow H \subseteq \mathbb{R}, \quad\; h = f(\mathbf{p}, \mathbf{y}, \mathbf{x}) = f(\mathbf{p}, \mathbf{g}(\mathbf{p}) - \mathbf{x}) = f(\mathbf{p}) \end{aligned} \tag{1}$$

where g and f are the functions defining the output variables (i.e., the model) and the objective function respectively. Both the functions have the design space P for the domain, while their ranges are $Y \subseteq \mathbb{R}^m$ for the output variable, and the solution space $H \subseteq \mathbb{R}$ for the objective function. Hence, in a single objective context the purpose of model calibration is to manipulate the values of **p** in order to drive the difference between simulated and observed values, y_j and x_j, to be as close to zero as possible. More formally, the aim of optimization is

$$\min_{\mathbf{p}} f(\mathbf{p}), \qquad \mathbf{p} \in P \subseteq \mathbb{R}^n. \tag{2}$$

Practically this involves finding an optimal parameter vector **p*** such than $f(\mathbf{p}^*) < f(\mathbf{p})$ for all $\mathbf{p} \in P$.

The calibration of hydrologic models often lends itself well to a multi-objective approach. An optimization problem is considered multi-objective if it contains more than one objective function. For z objective functions a multi-objective optimization problem can be formulated as

$$\min_{\mathbf{p}} (f_1(\mathbf{p}), f_2(\mathbf{p}), \ldots, f_z(\mathbf{p})), \qquad \mathbf{p} \in P \subseteq \mathbb{R}^n \tag{3}$$

where P is again the feasible domain of parameter vectors. Due to conflicting objectives, multi-objective optimization does not typically produce a single solution **p*** that would be optimal for all objectives simultaneously. Therefore, attention is instead paid to the Pareto optimal solutions. Such solutions are those where none of the objectives can be improved without deteriorating at least one of the other objectives. Thus a point in the feasible space **p*** is Pareto optimal if the vector of objective functions **f**(**p***) is non-dominated. The Pareto frontier is given by the set of the objective functions in the solution space whose vectors {**f(p**)} are non-dominated. The corresponding values of the model parameters {**p**} form the set of optimum solutions. The result of multi-objective calibration is an approximation of the true Pareto frontier, which could be reached in the limit if an infinite number of sample sizes could be evaluated. The parameter values of this approximated frontier represent trade-off solutions providing the best compromises among the various objectives.

2 VIC-GL Calibration Overview

Calibration of the VIC-GL model can be considered within the context of the water balance, which is given as

$$P(t) = R(t) + E(t) + \frac{dS_{sn}(t)}{dt} + \frac{dS_{gl}(t)}{dt} + \frac{dS_{sl}(t)}{dt} + \frac{dS_{gd}(t)}{dt} + \frac{dS_{lk}(t)}{dt} \quad (4)$$

where precipitation, *P*, into the basin at some time *t* is balanced by runoff, *R*, evapotranspiration, *E*, and changes in storage, *S*. Runoff includes all liquid water that exits a given domain as surface drainage and it usually considered the 'excess' component of the water budget. Evapotranspiration includes evaporation from the soil, evaporation of intercepted water from vegetation canopy, sublimation and transpiration. The final component of the water balance includes hydrologic fluxes created because of changes in snow (*sn*), glacier (*gl*), soil (*sl*), groundwater (*gn*) and lake (*lk*) storage. In order to ensure a robust and physically plausible model, it is desirable to explicitly target as many of the components of (4) as is feasible (i.e., for which data exists). Such an approach is ideally suited to a multi-objective calibration approach, wherein separate objectives are used to constrain the different components of the water balance.

Precipitation, which drives the hydrology model, is constrained as a measured input. Nevertheless, *P* has potentially large biases, particularly at high elevations (Adam and Lettenmaier 2003; Adam et al. 2006). Runoff, a spatially distributed quantity, is not directly observed and streamflow is used as a proxy. With the advent of new satellite-based measurements of various hydrological phenomena, additional data is now also available to constrain additional components of the water balance, including evapotranspiration, snow, and glacier storage (see Section 3). Groundwater (here representing large regional aquifers and water stored in bedrock as opposed to local soil water) is not modelled in VIC-GL and its significance in BC is not well quantified (although it may be a significant source of error in other regions, such as the southern Columbia and Prairies). Lake storage is also not explicitly modelled in VIC-GL and it's effect on model error has not been quantified.

The philosophy that governs the model calibration process is the desire to exploit the spatially distributed nature of the VIC-GL model. In an ideal setting, one would prefer to calibrate the model in a spatially explicit manner, i.e. grid cell by grid cell. However, as streamflow (or inflow) is typically the primary variable for water resources planning and management, the calibration design is dictated by the availability of discharge data. Hence, for calibration purposes the model domain is divided into sub-basins based on the location of hydrometric sites. This sub-division represents a trade-off between number of calibration sites and available record lengths; longer record lengths (but with fewer sites) include more hydro-climate variability to train the model robustly whereas more sites (with shorter records) allows for a more realistic spatial variability in the model parameters. We conduct calibration on each individual sub-basin, wherein model parameters are manipulated as spatially lumped quantities. The compromise is that spatial variability is maintained between sub-basins but is generally lost within sub-basins.

The results from preliminary calibration tests in several sub-basins were used to apply manual adjustments to parameters controlling transpiration and snow albedo decay (summarised in Table 1).

Early runs indicated that simulated evapotranspiration, ET, was generally too low in several test basins (Similkameen, Tulameen and Ashnola). As transpiration forms the largest proportion of ET, adjustments were made to leaf area index and minimum stomatal resistance values in the vegetation library to increase transpiration. Monthly leaf area index for all classes was scaled by a factor of 1.25 and minimum stomatal resistance was reduced by a factor of 3 (which reflects minimum 'canopy' resistance as opposed to the original 'stomatal' resistance values) (Kelliher et al. 1995). Parameters controlling the rate of snow albedo decay were also adjusted to reduce the rate of snow albedo decay over time, generally resulting in increased snow accumulation and delayed onset of snowmelt. Based on these initial tests it was also determined that the temperature lapse rate, instead of using a spatially varying climatological value (derived from ClimateWNA), should be adjusted during calibration from a base value of 7.5°C/1000m. This adjustment generally results in steeper temperature lapse rates throughout the study domain and stronger gradients in snow accumulation with elevation. These adjustments were applied globally to the entire model domain.

Due to the conflation of the glacier runoff signal with other runoff sources in streamflow data, the parameters controlling glacier runoff, GLAC_KMIN, GLAC_DK and GLAC_A (Table 1), were not calibrated for individual sub-basins. Instead, we used a single sub-basin, the Bridge River above La Joie Dam (BCHLJ; a heavily glaciated basin where discharge is considered very sensitive to glacier runoff) for calibration of these three parameters. Multi-objective calibration was carried out for BCHLJ and optimal values for the glacier runoff parameters were estimated using the average values from the best five runs. These optimal parameters values were than set globally for the entire study domain.

Modelled VIC-GL fluxes for all sub-basins were subsequently calibrated using the improved version of the non-dominated sorting genetic algorithm (NSGA-II) (Deb et al. 2002), an automatic evolutionary algorithm that solves the multiple objective global optimization problem. NSGA-II converges to and provides a sample of the Pareto frontier, which is a set of all parameter vectors that produce non-dominated values of the objective function vector. Implementation of the NSGA-II algorithm was accomplished using the *mco* R package (Mersmann 2014).

Table 1. VIC-GL Manual Calibration Parameters

Parameter	Adjustment	Value	Description
LAI	Scaling	1.25	Leaf area index
RMIN	Scaling	0.33	Minimum canopy resistance
SNOW_ALB_ACCUM_A	Absolute	0.95	Accumulation albedo decay parameter
SNOW_ALB_ACCUM_B	Absolute	0.40	Accumulation albedo decay parameter 2
SNOW_ALB_THAW_A	Absolute	0.85	Thaw albedo decay parameter
SNOW_ALB_THAW_B	Absolute	0.40	Thaw albedo decay parameter 2
TLAPSE	Absolute	7.50	Base temperature lapse rate (°C/km)
GLAC_KMIN	Absolute	0.05	Minimum glacier outflow factor
GLAC_DK	Absolute	0.50	Maximum increase in glacier outflow factor
GLAC_A	Absolute	15.00	Glacier outflow factor exponent

3 Automatic Calibration - Observed Data and Optimization Functions

3.1 Discharge

Streamflow data from various sources was used for calibration (Table 2). For regulated systems calibration was performed against naturalized discharge provided by BC Hydro, Rio Tinto Alcan and the BC Ministry of Environment (effects of regulation removed) and by the Bonneville Power Administration (Columbia basin; effects of regulation and irrigation removed). The calibration period for discharge was 1991 to 2000, a period that represents a trade-off between a sufficiently long calibration period and large enough number of stations to spatially discretize the study domain. This period captures substantial low-frequency variability over the region, capturing several ENSO cycles (Climate Prediction Centre NOAA 2015).

Table 2. Streamfow data sources

Data Source	Region	Conditions
Water Survey of Canada	Canada	Sites with unregulated discharge
United Sates Geological Survey	US	Sites with unregulated discharge
BC Hydro	BC	Naturalized discharge at BC Hydro generation sites in British Columbia (no regulation)
Rio Tinto Alcan	Nechako	Naturalized discharge for Nechako River sites regulated by the Nechako reservoir
BC Ministry of Environment	Fraser	Naturalized discharge for Fraser River sites regulated by the Nechako reservoir
Bonneville Power Administration	Columbia	Naturalized discharge in the Columbia basin (no regulation and no irrigation)

Estimation of streamflow at a specified gauge location (i.e., where measurements are available) requires parameterization of three sub-models: flux estimation (i.e., water balance calculation), grid cell routing, and channel routing. Grid cell fluxes of Runoff and Baseflow are estimated using the VIC-GL model whereas discharge is estimated using the RVIC routing model. During the calibration process only VIC-GL model parameters are adjusted. The routing parameters of the RVIC model were determined a priori and set globally and not adjusted as part of the calibration process. The routing parameters used in the current application are based on a previous calibration using gauging locations in the Fraser River basin (see Schnorbus et al. 2010) and the grid-cell unit hydrograph constructed using literature sources (see Appendix A). Hence, discharge calibration effectively calibrates the VIC-GL simulation of Runoff and Baseflow, where Runoff is strictly surface runoff and Baseflow is sub-surface runoff from soil storage.

The objective functions for discharge are chosen to constrain different aspects of the streamflow regime. For the current application of the VIC-GL model, three objective functions were used. The Kling-Gupta efficiency (KGE) goodness-of-fit measure was developed by Gupta et al. (2009) to provide diagnostic insight by decomposing model performance into correlation, bias and variability. The KGE is defined as

$$KGE = 1 - \sqrt{(r-1)^2 + (\alpha - 1)^2 + (\beta - 1)^2} \quad (5)$$

$$\alpha = \frac{\sigma_s}{\sigma_0}$$
$$\beta = \frac{\mu_s}{\mu_o}$$

where *r* is the linear correlation coefficient. Each of the terms in (5) have their optimum value at zero, such that the optimum KGE value is unity. From a hydrologic perspective usage of KGE makes sense, because in general we are interested in reproducing temporal dynamics (measured by *r*), as well as preserving the distribution of flows (flow duration curve), which can be summarized by the first and second moments (measured by α and β). Values for KGE range from one (perfect fit) to $-\infty$.

The Heteroscedastic Maximum Likelihood estimator (HMLE) (Sorooshian and Dracup 1980; Sorooshian et al. 1983) is the maximum likelihood, minimum variance, asymptotically unbiased estimator when the errors in the output data are Gaussian, zero mean, and uncorrelated and have nonstationary variance in time. The variance of the errors is assumed to be related to the level of the output (magnitude of the flows). Such errors are believed to be common in streamflow data. The HMLE is defined as

$$HMLE = \left\{\sum_{t=1}^{n} w_t \varepsilon_t^2\right\}\left\{n\left[\prod_{t=1}^{n} w_t\right]^{1/n}\right\}^{-1} \tag{6}$$

where $\varepsilon(t)$ is $y_s(t) - y_o(t)$, $w(t)$ is $f(t)^{2(\lambda-1)}$ and λ is the Box-Cox transformation parameter (Box and Cox 1964). The parameter λ is estimated by setting $f(t) = y_o(t)$ and optimizing for each new parameter vector using the `optimize` package in R (R Core Team 2016). The HMLE places greater weight on lower values, which are considered to have smaller errors and more information, than higher values.

A third objective function is the Nash-Sutcliffe Efficiency (NSE) (Nash and Sutcliffe 1970), defined as

$$NSE = 1 - \frac{\sum_{t=1}^{n}\{y_s(t) - y_o(t)\}^2}{\sum_{t=1}^{n}\{y_o(t) - \mu_o\}^2} \tag{7}$$

The NSE is essentially the mean squared error normalized by the standard deviation of observed values. NSE is as a classic skill score, where skill is interpreted as the comparative ability of a model with respect to a baseline model, which in this case is taken to be the mean of the observations. In this context if NSE ≤ 0 the model is no better than using the observed mean as a predictor. An NSE equal one indicates perfect model performance. In our calibration procedure, the NSE is applied using log-transformed discharge, which we call the LNSE objective (NSE of log-transformed discharge). The LNSE objective tends to place more uniform emphasis throughout the entire flow range and therefore tends to encourage parameter sets that have improved performance during recession and low flow periods.

Observed discharge at any location represents the total discharge generated by the entire upstream areas. For 2nd-order of higher sub-basins, VIC-GL runoff and baseflow integrate to produce local discharge only. Consequently, simulated local discharge must be combined with observed discharge flowing into the sub-basin from upstream sites prior to calibration. Unfortunately, the structure of the RVIC model does not allow the specification of in-channel flow as an upstream boundary condition.

Therefore, discharge ($m^3 s^{-1}$) from all upstream sites was converted to surface runoff ($mm\ d^{-1}$) and added to the appropriate cell in the flux file. However, as RVIC routes all runoff through the VIC cell prior to adding it to the channel network, the added runoff had to be reverse convolved of in-grid routing prior to adding it to the appropriate upstream VIC cell using the following procedure

$$r_c(t) = \left\{ \left[q_c(t) - \sum_{j=2}^{n} r_c(t-j+1) \cdot u(j) \right] u(1)^{-1} \right\} 86400 * 1000 / A_c \tag{8}$$

where *u* is the grid-cell unit hydrograph, *q* is discharge observed at upstream cell *c* and *A* is the area (m^2) of grid cell *c*. Reverse convolution is conducted at a daily time step using the daily unit hydrograph described in Table 3.

Table 3. Daily unit hydrograph used for reverse convolution

Day, *j*	u(*j*)
1	0.631978
2	0.328619
3	0.036218
4	0.003185

3.2 Evapotranspitation

Observed evapotranspiration data is provided by the LandFlux-EVAL multi-data set synthesis (Mueller et al. 2013). This data set is a monthly global synthesis of land evapotranspiration estimates from 14 global data sets for the period 1989 to 2005. The data sets can be categorized into three groups: diagnostic data derived from in situ or satellite-based observations, estimates calculated via land surface models driven with observation-based forcing, or estimates obtained as output from atmospheric reanalyses. The various products are merged and provided as set of gridded statistics (minimum, maximum, median, mean, 25th percentile, 75th percentile and standard deviation). The original merged product, which has a spatial resolution of 1°, was re-gridded to the spatial resolution of VIC-GL (1/16°) using distance-weighted average remapping using the `remapdis` function in cdo, (CDO 2015). The re-gridded product is then used to calculate basin-wide monthly values of the minimum, maximum and median ET (e_{min}, e_{max} and e_{med}, respectively).

Given that ET is provided as a range, we use a membership function to quantify how well simulated ET values, e_s, fall within the maximum-minimum range of the 'observed' basin-wide monthly ET data. Specifically, we employ an objective based on the bell-shaped membership function (Zhao and Bose 2002)

$$BMF_{ET} = \frac{1}{n} \sum_{t=1}^{n} \left\{ \frac{1}{1 + \left| \frac{e_s(t) - c(t)}{a(t)} \right|^{2b}} \right\} \tag{9}$$

where the width parameter, a, is set equal to $[e_{max}(t) – e_{min}(t)]/6$, the shape parameter, b, is set equal to a constant value of 2, and the parameter c, the centre of the curve, is set equal to $e_{med}(t)$. The bell function is smooth and non-zero at all points, with a maximum of one at e_{med}. Although the bell function does not equal zero for values below (above) the e_{min} (e_{max}), the function rapidly approaches zero beyond these limits. The BMF as defined is essentially the mean of the individual monthly membership calculations, with values ranging from one (best) to zero (worst). The calibration period for monthly ET is identical to that of streamflow, which is 1991 to 2000 (n = 120).

3.3 Snow Covered Area

Snow covered area (SCA) data is used to constrain the snow accumulation and melt process in VIG-GL. Observed snow covered area (SCA) is provided by the MODIS/Terra Snow Cover Monthly L3 Global 0.05Deg CMG, Version 6 (MOD10CM) (Hall and Riggs 2015). The MOD10CM product is a satellite-based global estimate of SCA based on the Normalized Difference Snow Index (NDSI). SCA is given as a snow cover fraction for each 0.05° grid. A time series of basin-wide monthly SCA for each sub-basin was produced by taking the weighted average of the overlapping 0.05° grids for each month. Area averages were calculated using the `extract` function from the *raster* R package (Hijmans 2016), using normalized weights based on the fraction of each cell within the sub-basin. The calibration period for SCA is January 2001 to December 2005 (n = 60). We use the KGE as the objective function for assessing SCA.

3.4 Glacier Mass Balance

For glaciated basins, an additional constraint was imposed by calibrating to glacier mass balance data. Observations were the geodetic thinning rates, ΔH, estimated for the period 1985 to 1999 by Schiefer et al. (2007). Thinning rates were provided as a basin-wide annual average, obtained by averaging a 100-m resolution difference grid over the glaciated regions of each sub-basin (as defined by the 1/16° sub-basin boundaries) and averaging over the measurement period (n=15 years). Uncertainty in the thinning rate was estimated as ±3.0 m for the observation period, based on a BC-wide standard error estimate of ±0.19 m/a reported by Schiefer et al. (2007). Thickness changes were converted to water equivalent using an area-weighted density for firn (550 kg m^{-3}) in the accumulation zone and ice (910 kg m^{-3}) in the ablation zone. Area weighting used accumulation area ratios of 0.15 to 0.6 (conversion factors of 0.85 to 0.7) (B. Menounos, personal communication). The lower and upper estimate of measured geodetic mass balance in water equivalent were then estimated as

$$\begin{aligned} b_l &= min\,\{0.7(\Delta H - 3), 0.85(\Delta H - 3)\} \\ b_u &= max\{0.7(\Delta H + 3), 0.85(\Delta H + 3)\} \end{aligned} \tag{10}$$

with a 'mid-point' estimate calculated as

$$b_m = (b_u - b_l)/2. \tag{11}$$

We use the following bell membership function to assess model performance

$$BMF_B = \frac{1}{1 + \left|\frac{b_s - b_m}{(b_u - b_l)}\right|^2}. \tag{12}$$

3.4.1 Multi-objective Optimization Function

The generic multi-objective problem specified by (3) now becomes

$$\min_{\mathbf{p}}\left(f_1(\mathbf{p}), f_2(\mathbf{p}), f_3(\mathbf{p}), f_4(\mathbf{p}), f_5(\mathbf{p}), f_6(\mathbf{p})\right), \qquad \mathbf{p} \in P \subseteq \mathbb{R}^n \tag{13}$$

where f_1 = -KGE_Q, f_2 = $HMLE_Q$, f_3 = -$LNSE_Q$, f_4 = -BMF_{ET}, f_5 = -KGE_{SCA}, and f_6 = 1_G(-BMF_B), where 1_G is equal 1 if glacier area > 0 km^2 and equal 0 otherwise. Note the use of negative signs for KGE, BMF, and LNSE to accommodate function minimization. Subscripts *Q*, *ET*, *SCA* and *B* refer to discharge, evapotranspiration, snow cover area, and glacier mass balance, respectively. The feasible parameter domain is defined using parameter ranges for individual elements of the vector **p** (see Section 4).

3.5 Forcing Data

During model calibration, VIC-GL was forced using a gridded meteorological data set produced specifically for the 2nd generation modelling. This data set contains daily observations gridded at 1/16° (same spatial resolution as VIC-GL) with the variables of maximum and minimum temperature, precipitation and average wind speed. The temperature and precipitation variables were gridded via thin-plate spline interpolation of station data using and a 30-year climatology based on ClimateWNA as a covariate. The wind speed observations were downscaled from the 20th Century Reanalysis, versions 2 (20CR v2; Compo et al. 2011) via bi-linear interpolation. Werner et al. (in press) provides more details on the forcing data.

4 VIC-GL Model Parameters

Most VIC-GL parameters are treated as 'observed' and not modified during the calibration process. Only a small set of model parameters are used to calibrate the model, chosen either because they are the most sensitive parameters (Demaria et al. 2007) or the they tend to reflect the more empirical aspects of the model (and as such may not have a physically measurable meaning). The VIC-GL parameters selected for adjustment during automatic calibration are described in Table 4. For each iteration of the calibration process, a parameter vector $\Theta = \{\theta_1, \theta_2, \dots, \theta_k\}$ was sampled by adjusting the individual elements of a base parameter vector $\Phi = \{\phi_1, \phi_2, \dots, \phi_k\}$ using three possible procedures (depending upon the parameter):

- Absolute – original value replaced with $\theta_i = p_i$
- Scaling – original value multiplicatively scaled as $\theta_i = p_i \phi_i$
- Delta – original value additively scaled as $\theta_i = p_i + \phi_i$

where $\{p_1, p_2, \dots, p_k\}$ is a random vector sampled from the ranges given in Table 4. Parameter adjustments, p, were constrained to a precision of 0.001, except *BI* and *DS* that used a precision of 0.0001.

Table 4. VIC-GL Automated Calibration Parameters

Parameter	Adjustment	Range‡	Description (with units where applicable)
BI	Absolute	0.5000 - 0.0001	Infiltration partitioning parameter
DS	Absolute	0.2000 - 0.0001	Baseflow curve parameter
DSMAX	Scaling	2.000 - 0.001	Maximum baseflow
WS	Absolute	0.950 - 0.200	Baseflow curve parameter
EXPN	Scaling	3.000 - 1.000	Vertical change in hydraulic conductivity in all soil layers
D3	Scaling	3.000 - 0.500	Depth of third soil layer
NEWALB	Absolute	0.950 - 0.850	Albedo of new snow
PADJ_R	Absolute	2.000 - 0.250	Precipitation adjustment for rainfall
PADJ_S	Absolute	2.000 - 0.250	Precipitation adjustment for snowfall
TLAPSE	Delta	2.500 - -2.500	Temperature lapse rate (°C/km)
GLACALB	Absolute	0.600 - 0.200	Glacier albedo (when $1_G = 1$)
GLACRF	Absolute	1.000 - 0.000	Snow redistribution to glaciers (when $1_G = 1$)

‡ Precision reflected by number of decimal places in the range values

The *BI* parameter controls the partitioning of net precipitation or snowmelt into surface (or quick) runoff and infiltration (which ultimately becomes evaporation, transpiration or baseflow). The *DS* and *WS* parameters control the shape of the baseflow curve (specifically the location of the inflection point from where baseflow transitions from a linear to a non-linear function of soil moisture). *DSMAX* specifies the maximum baseflow velocity and base values are set as a function of local slope. This parameter is adjusted using the scaling approach in order to maintain the original spatial variability. The *EXPN* parameter (one per soil layer) describes the exponential change of hydraulic conductivity with depth. A nominal base value is estimated as 3+2/*L*, where *L* is the pore size index (which is a function of soil texture). The EXPN parameter is adjusted by using the same scaling factor for each soil layer. *D3* is the depth of the third soil layer, with nominal base values estimated as a function of local elevation and slope. Values for *D3* are scaled during calibration to maintain the original underlying spatial variability. *NEWALB* is the albedo of new fallen snow. *PADJ_R* and *PADJ_S* are precipitation adjustment factors for rainfall and snowfall, respectively. *TLAPSE* is the temperature lapse rate in each grid cell. Although a base value was originally estimated per cell, using local temperature gradients estimated from Climate WNA, preliminary testing indicated that a global base value of 7.5°C/1000m was more effective. *GLACALB* is the albedo of glacier ice. *GLACRF* is a parameter that controls the redistribution of snowfall between non-glacier and glacier HRUs per elevation band.

It is recognized that the use of separate precipitation adjustment parameter for rain and snow may introduce artefacts in the climate change projections. For forcing the hydrologic simulations, only precipitation is downscaled from the driving global climate experiment, and the partitioning into rain and snow is estimated in VIC-GL (using air temperature thresholds). Hence, under future climates the precipitation trend supplied by a GCM will be partitioned into separate rain and snow trends by VIC-GL, depending on the temperature trend (i.e. rainfall may increase and snowfall may decrease). Consequently, applying independent precipitation adjustments to rain and snow may inadvertently produce a precipitation trend in VIC-GL that differs from that in the driving climate experiment. Therefore, in practice the PADJ_R and PADJ_S parameters are always set equal during model calibration.

5 Parameter Selection

Once the final set {**p**} of optimum solutions has been generated, typically only one solution from this set is selected for model projections. The process of parameter selection is conducted in two stages. The first stage is to adopt a fuzzy approach to ranking the parameter vectors in the Pareto optimum solution. For a given parameter vector, **p**, a fuzzy score is calculated as the weighted-average of individual membership values for each normalized objective function value as

$$S = \sum_{r=1}^{z} w_r \, \mu_r(\tilde{f}_r(\mathbf{p})) \qquad \mathbf{p} \in P \subseteq \mathbb{R}^n \tag{14}$$

where $\tilde{f}_r(\mathbf{p})$ is $f_r(\mathbf{p})$ normalized to the range (0,1), $\mu_r(\cdot)$ is the sigmoidal membership function

$$\mu_r(x; a, b) = \frac{1}{1 + e^{-a_r(x-b_r)}}, \tag{15}$$

where *a* determines the steepness of the function (if *a* is negative the function is open to the left) and *b* locates the value of *x* where μ_r = 0.5, and *w* is the weight given to each objective function, where $\sum_r w_r = 1.0$. The parameter values for equations (14) and (15) are given in Table 5.

Table 5. Parameter values for Fuzzy Score calculation

Objective	Parameter value with (without) glaciers		
	a	*b*	*w*
$-KGE_Q$	-20	0.25	0.3 (0.4)
$HMLE_Q$	-10	0.5	0.1 (0.1)
$-LNSE_Q$	-10	0.5	0.3 (0.3)
$-BMF_{ET}$	-10	0.5	0.05 (0.1)
$-KGE_{SCA}$	-10	0.5	0.05 (0.1)
$-BMF_B$	-20	0.25	0.2 (0.0)

For the second stage of parameter selection, the final performance scores are ranked and the top ten vectors are selected for further evaluation. The second evaluation stage involves a heuristic assessment of model performance, based on a visual assessment of a number of different chart types (see Figure 2 through Figure 7 for examples), plus a deeper inspection of additional metrics not used in the automated calibration process. The final parameter set is the one subjectively chosen as the 'best'.

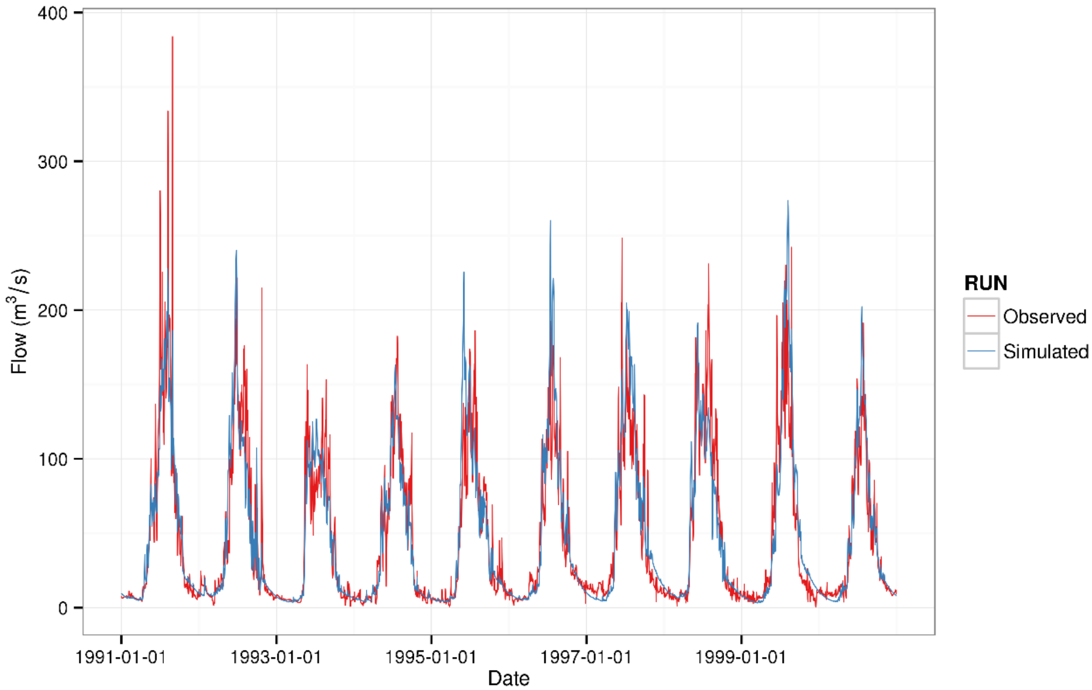

Figure 1. Example daily calibration period hydrograph for BCHLJ

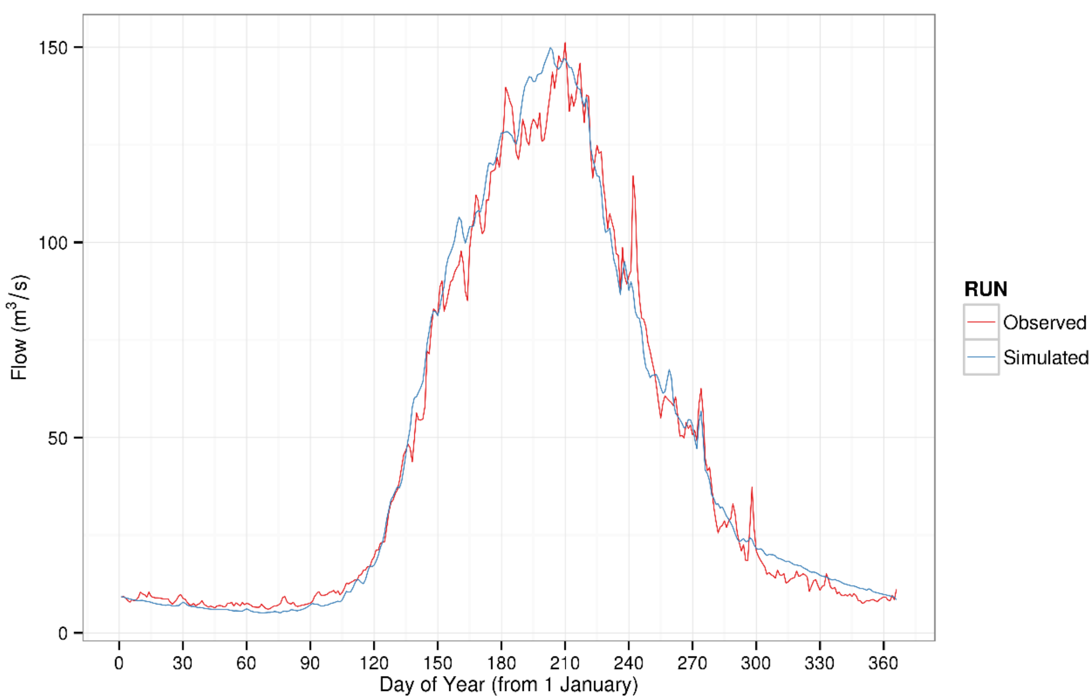

Figure 2. Climatological daily calibration period hydrograph for BCHLJ

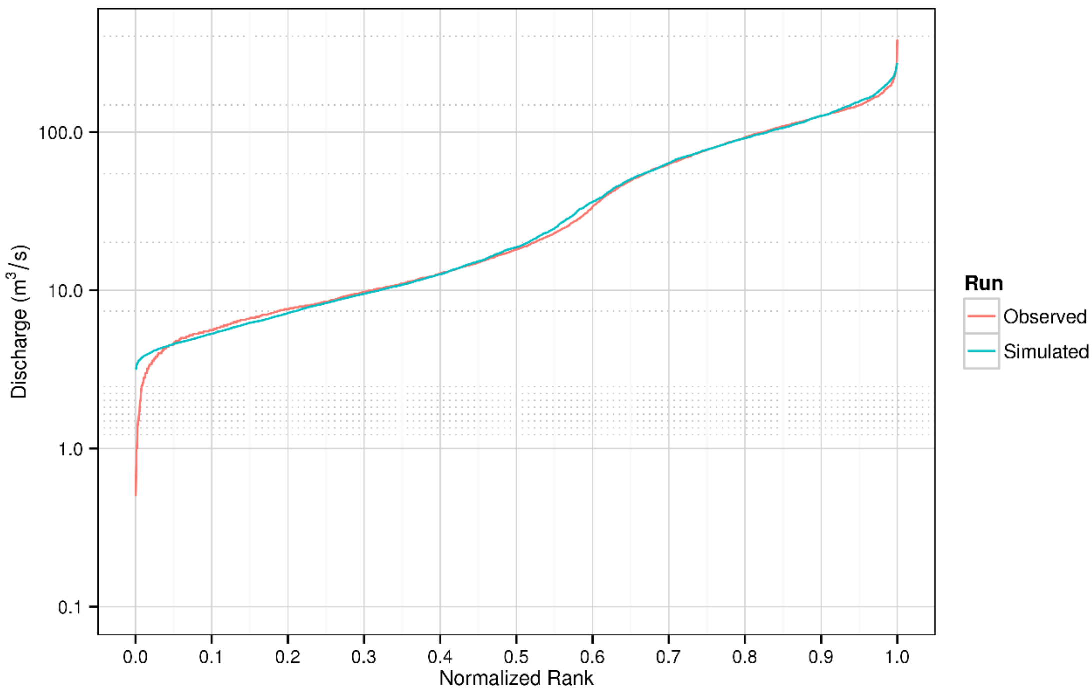

Figure 3. Calibration period flow duration curve for BCHLJ

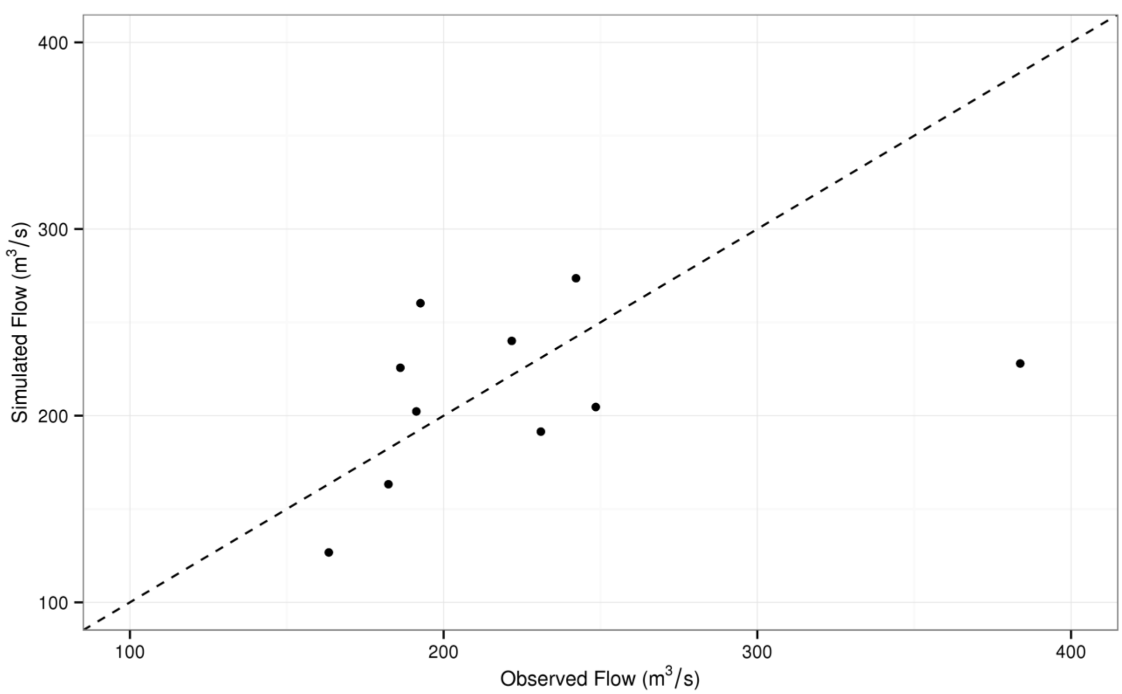

Figure 4. Calibration period annual maximum peak flow scatterplot for BCHLJ

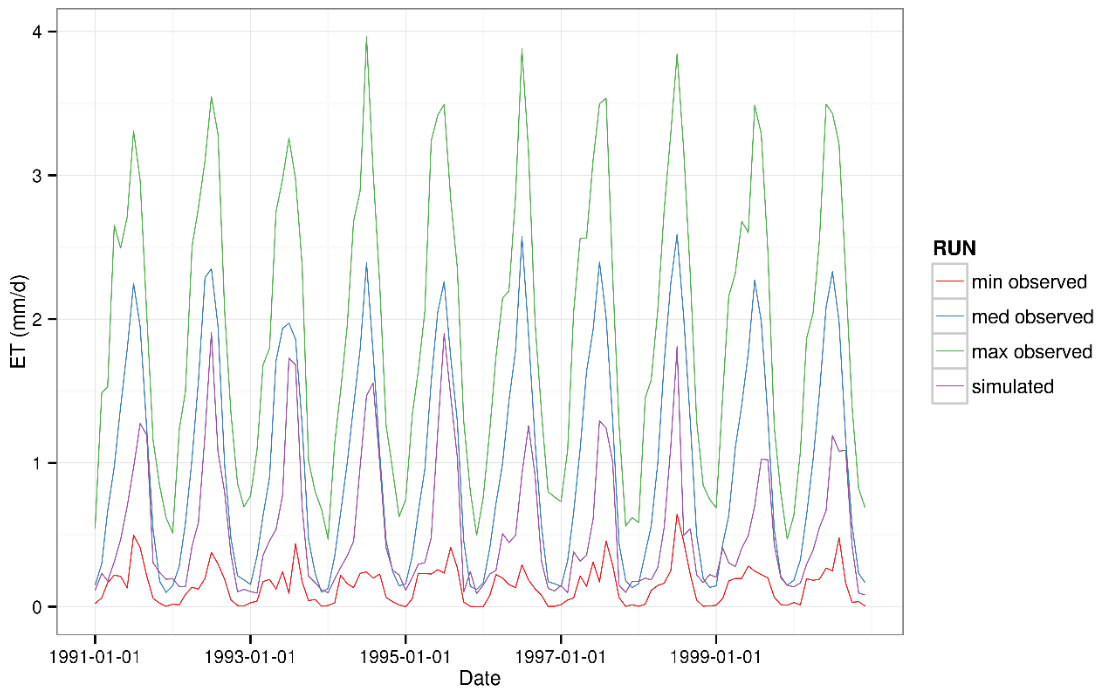

Figure 5. Calibration period monthly evapotranspiration for BCHLJ.

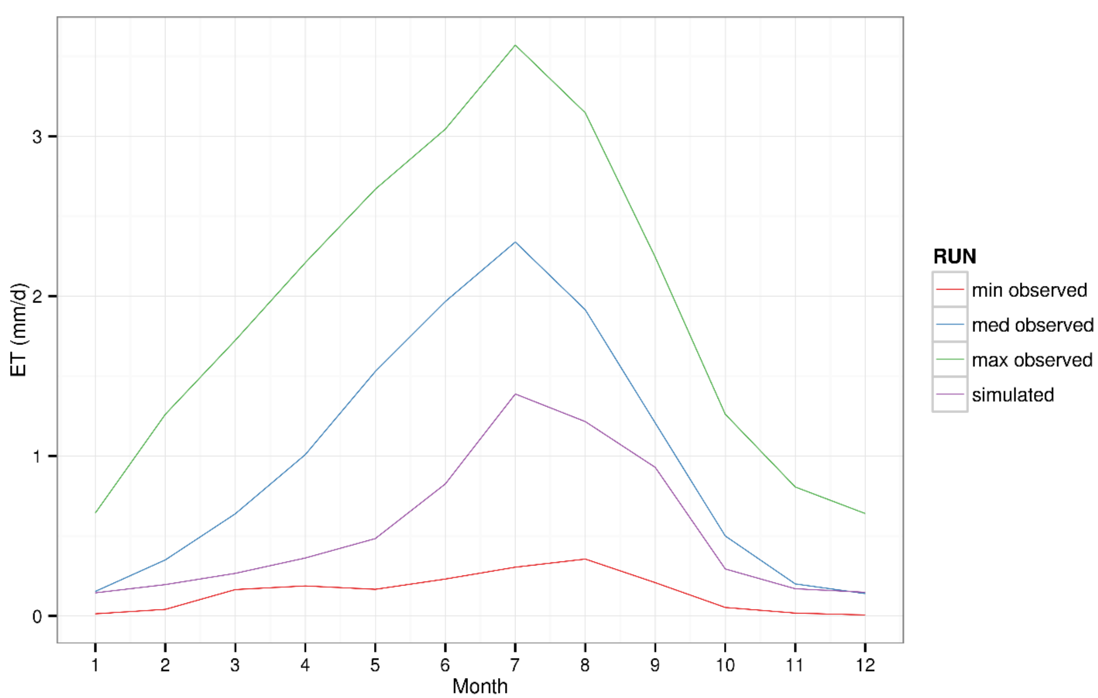

Figure 6. Calibration period climatological monthly evapotranspiration for BCHLJ.

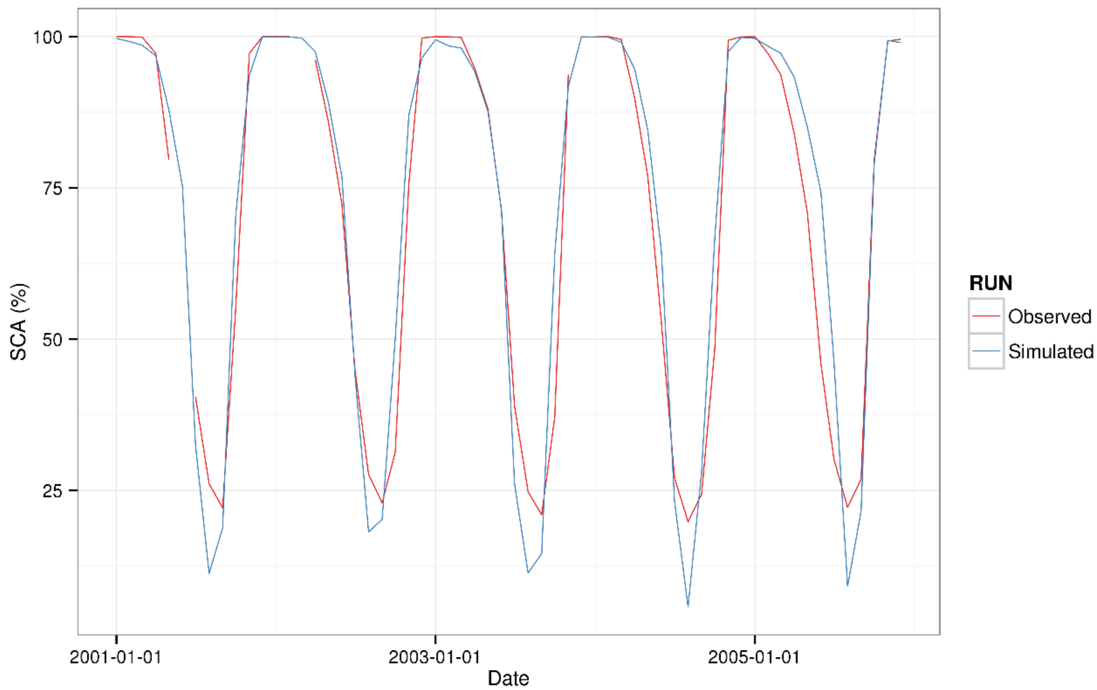

Figure 7. Calibration period monthly snow cover area fraction for BCHLJ.

6 References

Adam, J. C., and D. P. Lettenmaier, 2003: Adjustment of global gridded precipitation for systematic bias. *J. Geophys. Res.-Atmospheres*, **108**, doi:4257 10.1029/2002jd002499.

Adam, J. C., E. A. Clark, D. P. Lettenmaier, and E. F. Wood, 2006: Correction of Global Precipitation Products for Orographic Effects. *J. Clim.*, **19**, 15–38, doi:Article.

Arcement Jr., G. J., and V. R. Schneider, 1989: *Guide for Selecting Manning's Roughness Coefficients for Natural Channels and Flood Plains*. United States Geological Survey, US, http://pubs.er.usgs.gov/publication/wsp2339.

Box, G. E. P., and D. R. Cox, 1964: An Analysis of Transformations. *J. R. Stat. Soc. Ser. B Methodol.*, **26**, 211–252.

Bras, R. L., 1990: *Hydrology: An introduction to hydrologic science*. Addison-Wesley Publishing Company, Reading, MA, 643 pp.

Cavazzuti, M., 2013: *Optimization Methods - From Theory to Design*. Springer-Verlag, Berlin, 262 pp.

CDO, 2015: *Climate Data Operators*. http://www.mpimet.mpg.de/cdo.

Climate Prediction Centre NOAA, 2015: Cold and warm episodes by season. *Hist. El Nino Nina Episodes 1950-Present*,. http://www.cpc.ncep.noaa.gov/products/analysis_monitoring/ensostuff/ensoyears.shtml (Accessed June 2, 2017).

Compo, G. P., and Coauthors, 2011: The Twentieth Century Reanalysis Project. *Q. J. R. Meteorol. Soc.*, **137**, 1–28, doi:10.1002/qj.776.

Cudworth Jr., A. G., 1989: *Flood Hydrology Manual*. First. United States Department of Interior, Bureau of Reclamation, Denver, CO, 243 pp.

Deb, K., A. Pratap, S. Agarwal, and T. Meyarivan, 2002: A fast and elitist multiobjective genetic algorithm: NSGA-II. *IEEE Trans. Evol. Comput.*, **6**, 182–197, doi:10.1109/4235.996017.

Demaria, E. M., B. Nijssen, and T. Wagener, 2007: Monte Carlo sensitivity analysis of land surface parameters using the Variable Infiltration Capacity model. *J. Geophys. Res.-Atmospheres*, **112**, doi:D11113 10.1029/2006jd007534. ://WOS:000247369100001.

Gupta, H. V., H. Kling, K. K. Yilmaz, and G. F. Martinez, 2009: Decomposition of the mean squared error and NSE performance criteria: Implications for improving hydrological modelling. *J. Hydrol.*, **377**, 80–91, doi:10.1016/j.jhydrol.2009.08.003.

Hall, D. K., and G. A. Riggs, 2015: MODIS/Terra Snow Cover Monthly L3 Global 0.05Deg CMG, Version 6. doi:http://dx.doi.org/10.5067/MODIS/MOD10CM.006.

Hijmans, R. J., 2016: *raster: Geographic Data Analysis and Modeling*. https://CRAN.R-project.org/package=raster.

Kelliher, F. M., R. Leuning, M. R. Raupach, and E.-D. Schulze, 1995: Maximum conductances for evaporation from global vegetation types. *Agric. For. Meteorol.*, **73**, 1–16, doi:10.1016/0168-1923(94)02178-M.

Loader, C., 2013: *locfit: Local regression, likelihood and density estimation*. https://CRAN.R-project.org/package=locfit.

Mersmann, O., 2014: *mco: Multiple Criteria Optimization Algorithms and Related Functions*. https://CRAN.R-project.org/package=mco.

Mueller, B., and Coauthors, 2013: Benchmark products for land evapotranspiration: LandFlux-EVAL multi-data set synthesis. *Hydrol Earth Syst Sci*, **17**, 3707–3720, doi:10.5194/hess-17-3707-2013.

Nash, J. E., and J. V. Sutcliffe, 1970: River flow forecasting through conceptual models. Part I - discussion of principles. *J. Hydrol.*, **10**, 282–290.

R Core Team, 2016: *R: A Language and Environment for Statistical Computing*. R Foundation for Statistical Computing, Vienna, Austria, http://www.R-project.org/.

Schiefer, E., B. Menounos, and R. Wheate, 2007: Recent volume loss of British Columbian glaciers, Canada. *Geophys. Res. Lett.*, **34**, L16503, doi:10.1029/2007GL030780.

Schnorbus, M., K. Bennett, and A. Werner, 2010: *Quantifying the water resource impacts of mountain pine beetle and associated salvage harvest operations across a range of watershed scales: Hydrologic modelling of the Fraser River basin.* Canadian Forest Service, Pacific Forestry Centre, Victoria, B.C., http://www.cfs.nrcan.gc.ca/pubwarehouse/pdfs/31207.pdf.

Sorooshian, S., and J. A. Dracup, 1980: Stochastic parameter estimation procedures for hydrologic rainfall-runoff models: Correlated and heteroscedastic error cases. *Water Resour. Res.*, **16**, 430–442, doi:10.1029/WR016i002p00430.

——, V. K. Gupta, and J. L. Fulton, 1983: Evaluation of Maximum Likelihood Parameter estimation techniques for conceptual rainfall-runoff models: Influence of calibration data variability and length on model credibility. *Water Resour. Res.*, **19**, 251–259, doi:10.1029/WR019i001p00251.

Werner, A. T., M. A. Schnorbus, R. R. Shrestha, A. J. Cannon, F. W. Zwiers, G. Dayon, and F. Anslow, in press: A long-term, temporally consistent, gridded daily meteorological dataset for northwest North America. *Sci. Data*,.

Zhao, J., and B. K. Bose, 2002: Evaluation of membership functions for fuzzy logic controlled induction motor drive. *IECON 02 [Industrial Electronics Society, IEEE 2002 28th Annual Conference]*, Vol. 1 of, IECON 02 [Industrial Electronics Society, IEEE 2002 28th Annual Conference], Sevilla, Spain, IEEE, 229–234 vol.1.

Appendix A – Grid Cell Unit Hydrograph

The RVIC routing model uses an hourly unit hydrograph per grid cell that describes the routing of within-cell surface water to the grid cell outlet (i.e., to the main channel). For practical purposes, a single hourly unit hydrograph is prescribed for the entire modelling domain. This cell unit hydrograph was been estimated using the Soil Conservation Service (SCS) dimensionless unit hydrograph procedure (e.g. Bras 1990). The dimensionless unit hydrograph, which is the result of averaging a large number of individual dimensionless unit hydrographs, has a time-to-peak located at approximately 20% of its time base and an inflection point at 1.7 times the time-to-peak. The dimensionless hydrograph describes the evolution of discharge using the time ratio, t/t_p and discharge ratio, q/q_p, where t_p is time to peak and q_p is peak discharge. Table A1 provides the ratios for the dimensionless unit hydrograph and the corresponding mass curve (*Unit Hydrograph (UHG) Technical Manual*, National Weather Service - Office of Hydrology Hydrologic Research Laboratory & National Operational Hydrologic Remote Sensing Center; http://www.nohrsc.noaa.gov/technology/gis/uhg_manual.html).

The time axis of the dimensionless hydrograph was scaled using an estimated time to peak (Bras 1990)

$$t_p = \frac{D}{2} + t_L \qquad (16)$$

where D is the duration of effective rainfall (in this case interpreted as daily) and t_L is the lag time, calculated as (Cudworth Jr. 1989)

$$t_L = 26 \cdot K_n \left(\frac{L \cdot L_c}{S^{0.5}}\right)^{0.33} \qquad (17)$$

where L is the distance of the longest watercourse (in miles), L_c is the distance from the basin centroid to the outlet, S is the overall slope of L (in feet per mile) and K_n is a weighted value of Manning's roughness coefficient. The value for K_n is computed by (Arcement Jr. and Schneider 1989)

$$K_n = (n_b + n_1 + n_2 + n_3 + n_4)m \qquad (18)$$

where n_b is a base Manning's value for a straight uniform smooth, channel in natural materials, n_1 is a correction factor for the effect of surface irregularities, n_2 is a value for variations in shape and size of the channel cross section, n_3 is a value for obstructions, n_4 is a value for vegetation and flow conditions, and m is a correction factor for meandering of the channel. Arcement Jr. and Schneider (1989) provide guidance for setting values of the various parameters in (18) for a range of conditions and channel types, and these have been set to represent generic conditions, summarized in Table A2, for small headwater channels located in mountainous topography.

Table A1. Ratios for dimensionless unit hydrograph and mass curve

Time Ratios (t/t_p)	Discharge Ratios (q/q_p)	Mass Curve Ratios (Q_a/Q)
0.0	0.000	0.000
0.1	0.030	0.001
0.2	0.100	0.006
0.3	0.190	0.012
0.4	0.310	0.035
0.5	0.470	0.065
0.6	0.660	0.107
0.7	0.820	0.163
0.8	0.930	0.228
0.9	0.990	0.300
1.0	1.000	0.375
1.1	0.990	0.450
1.2	0.930	0.522
1.3	0.860	0.589
1.4	0.780	0.650
1.5	0.680	0.700
1.6	0.560	0.751
1.7	0.460	0.790
1.8	0.390	0.822
1.9	0.330	0.849
2.0	0.280	0.871
2.2	0.207	0.908
2.4	0.147	0.934
2.6	0.107	0.953
2.8	0.077	0.967
3.0	0.055	0.977
3.2	0.040	0.984
3.4	0.029	0.989
3.6	0.021	0.993
3.8	0.015	0.995
4.0	0.011	0.997
4.5	0.005	0.999
5.0	0.000	1.000

Values for the remaining parameters have been chosen to reflect the fact that the SCS procedure is being used to describe surface routing within individual VIC cells, hence distances generally reflect the size of the VIC cells at the approximate centre of the PCIC modelling domain (55°N latitude). For a model spatial resolution of 1/16-degree the final values are D=24 hours (routing time step is daily), L = 6 km (3.73 mi), L_c = L/2 = 3km (1.86 mi), and S = 5%, resulting in t_L = 6 hours and t_p = 18 hours.

Table A2. Parameter values for Manning's roughness

Parameter	Value	Description
n_b	0.040	Base roughness - cobble-boulder bed
n_1	0.008	Irregularity – moderate
n_2	0.003	Cross section variation – alternating occasionally
n_3	0.020	Obstructions - appreciable
n_4	0.002	Amount of vegetation – small
m	1.000	Degree of meandering – minor
K_n	0.073	Effective Manning's value

The relationship between t/t_p and q/q_p given in Table A1 was fit using local polynomial regression (*locift* R package; Loader (2013)) using a second-degree polynomial and a smoothing parameter of 0.2. This fitted model was then used to predict q/q_p values at the required values of t/t_p corresponding to every whole hour from t = 0, 1, …, T (where T = 96 hours and t_p is as calculated). The final unit hydrograph is calculated by normalizing the dimensionless hydrograph using

$$q_n(t) = \left[\frac{q(t)}{q_p}\right]\left[\sum_{t=1}^{T}\frac{q(t)}{q_p}\right]^{-1} \quad (19)$$

The final VIC cell unit hydrograph is given in Figure A1. It is noted that the final hourly unit hydrograph is somewhat unrealistic in that runoff peaks and declines at ~18 hours, despite that fact that the duration of 'effective rainfall' is 24 hours. In other words, it would be more realistic for the hydrograph to peak at ~18-hours and remain plateaued until the cessation of rainfall (at 24 hours) and then decline. This represents a shortfall in the SCS dimensionless hydrograph approach for large durations, D. Nevertheless, the unit hydrograph produced is sufficiently accurate for estimating daily discharge.

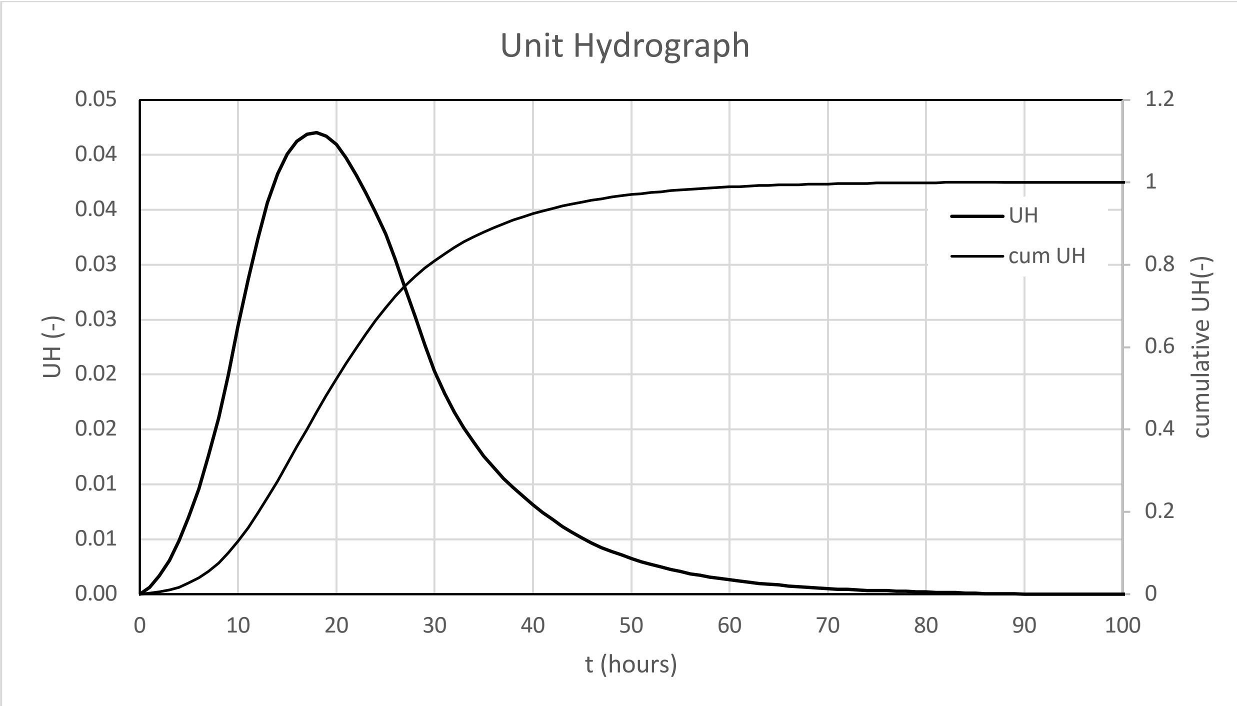

Figure A1. Grid cell unit hydrograph (UH) and cumulative unit hydrograph (cum UH).